Quality and compatibility analyses of global aerosol products derived from the advanced very high resolution radiometer and Moderate Resolution Imaging Spectroradiometer

Myeong-Jae Jeong,[1] Zhanqing Li,[1,2] D. Allen Chu,[3,4] and Si-Chee Tsay[5]

Received 15 February 2004; revised 16 August 2004; accepted 5 October 2004; published 1 March 2005.

[1] There exist numerous global aerosol products derived from various satellite sensors, but little insight has been gained about their compatibility and quality. This study presents a comparison of two prominent global aerosol products derived over oceans from the advanced very high resolution radiometer (AVHRR) under the Global Aerosol Climatology Project (GACP) (Mishchenko et al., 1999) and the Moderate Resolution Imaging Spectroradiometer (MODIS) (Tanré et al., 1997). The comparisons are for monthly mean aerosol optical thickness (AOT) and Ångström exponent (α) at a spatial resolution of 1×1 degree. The two monthly AOT products showed substantial discrepancies, with a tendency of higher values from MODIS than from GACP/AVHRR, especially near the coasts of major aerosol outbreak regions. Individual monthly AOT values have poor correlation, but their regional means are moderately correlated (correlation coefficient $0.5 < R < 1.0$). While cloud screening has often been argued to be a major factor explaining large discrepancies, this study shows that differences in aerosol models in the two retrieval algorithms can lead to large discrepancies. Contributions of the size distribution are more significant than the refractive index. The noisiness of the GACP/AVHRR aerosol retrievals seem to be partially influenced by radiometric uncertainties in the AVHRR system, but it is unlikely a major factor to explain the observed systematic discrepancies between the MODIS and GACP/AVHRR AOTs. For α, correlations between MODIS and GACP/AVHRR are lower ($0.2 < R < 0.7$) than AOT. The MODIS α shows a well-behaved dependence on the AOT contingent upon the aerosol type, while the GACP/AVHRR α has little correlation with the AOT. The high sensitivity in the selection of aerosol models to radiometric errors may be a primary reason for the worse comparison of α. Part of the discrepancies in α is attributed to different aerosol size distributions.

Citation: Jeong, M.-J., Z. Li, D. A. Chu, and S.-C. Tsay (2005), Quality and compatibility analyses of global aerosol products derived from the advanced very high resolution radiometer and Moderate Resolution Imaging Spectroradiometer, *J. Geophys. Res.*, *110*, D10S09, doi:10.1029/2004JD004648.

1. Introduction

[2] Satellite-based remote sensing plays a vital role in gaining a good knowledge and understanding of global aerosol variations and interaction with the Earth's climate [*Kaufman et al.*, 2002]. While satellite data have long been employed for aerosol studies, major challenges still confront us in almost every step of the retrieval process, namely, sensor calibration, cloud screening, corrections for surface reflectivity and variability of aerosol properties (size distribution, refractive index, etc.) [*King et al.*, 1999]. Consequently, significant differences exist among various aerosol products generated from the AVHRR [*Stowe et al.*, 1997; *Higurashi and Nakajima*, 1999; *Mishchenko et al.*, 1999; *Ignatov and Stowe*, 2002a; *Ignatov et al.*, 2004], the MODIS [*Tanré et al.*, 1997; *Kaufman et al.*, 1997; *Remer et al.*, 2005], the Total Ozone Mapping Spectrometer (TOMS) [*Herman et al.*, 1997; *Torres et al.*, 1998, 2002], the Polarization and Directionality of the Earth's Reflectances (POLDER) instrument [*Goloub et al.*, 1999; *Deuzé et al.*, 2000], and the Multiangle Imaging Spectroradiometer (MISR) [*Kahn et al.*, 1998, 2001], etc. *Myhre et al.* [2004] compared a large number of global aerosol products and revealed the general features of agreement and discrepancies, but insights into the causes for the discrep-

[1]Department of Meteorology and Earth System Science Interdisciplinary Center, University of Maryland, College Park, Maryland, USA.
[2]Also at Institute of Atmospheric Physics, Chinese Academy of Sciences, Beijing, China.
[3]Joint Center for Earth Science and Technology, University of Maryland, Baltimore, Maryland, USA.
[4]Also at Laboratory for Atmospheres, NASA Goddard Space Flight Center, Greenbelt, Maryland, USA.
[5]Laboratory for Atmospheres, NASA Goddard Space Flight Center, Greenbelt, Maryland, USA.

0148-0227/05/2004JD004648$09.00

ancies were lacking and the state-of-the-art aerosol product from the MODIS was excluded from their work.

[3] This study conducts a more detailed comparison of aerosol products over oceans from two prominent sensors: MODIS and AVHRR [*Tanré et al.*, 1997; *Mishchenko et al.*, 1999]. Possessing the longest satellite record, AVHRR data have been employed in studying long-term variations of atmospheric aerosols [*Mishchenko et al.*, 2003]. Using various retrieval algorithms, aerosol optical thickness (AOT) was inferred from reflectances measured at a single channel [*Rao et al.*, 1989; *Stowe et al.*, 1997; *Ignatov et al.*, 2004], and at multiple channels [e.g., *Higurashi and Nakajima*, 1999; *Mishchenko et al.*, 1999; *Ignatov and Stowe*, 2002a]. In some algorithms, an additional parameter (often the Ångström exponent) was also estimated. So far, all global aerosol products generated from the AVHRR have been confined to oceans primarily due to difficulties in separating aerosol signals from those from land surfaces of high reflectivity [*King et al.*, 1999]. Taking advantage of a unique relationship between reflectances at longer and shorter wavelengths available from the MODIS, *Kaufman et al.* [1997] proposed a method that extends the retrieval of the AOT over the majority of land areas except over bright desert or barren land. Note that a different algorithm was used to retrieve the AOT over oceans [*Tanré et al.*, 1997]. Validations of the MODIS AOT retrievals against ground-based Aerosol Robotic Network (AERONET) [*Holben et al.*, 1998, 2001] observations showed good accuracies over both oceans and land [*Remer et al.*, 2002; *Chu et al.*, 2002].

[4] In addition to the AOT, the Ångström exponent (α) [*Ångström*, 1929, 1964] has been widely used for various applications by virtue of its relationship to aerosol size. For instance, α is used for interpolation (or extrapolation) of aerosol optical thickness (AOT) at a certain wavelength [e.g., *Kinne et al.*, 2001; *Myhre et al.*, 2004] and is used as a proxy of particle size when direct measurements of aerosol particle size (effective, mean or mode radius, etc.) are not available [*Chou et al.*, 2002; *Sakerin and Kabanov*, 2002; *Moorthy et al.*, 2003]. *Nakajima et al.* [2001] used α to study the aerosol indirect effect which is defined as the radiative forcing associated with the modification of cloud microphysics due to aerosols [*Twomey et al.*, 1984; *Coakley et al.*, 1987; *Charlson et al.*, 1992]. Note that α depends on the wavelengths for which it is derived.

[5] Retrievals of AOT and α are affected by aerosol size distributions and optical properties. Numerous studies reported diverse optical and physical properties of aerosols [e.g., *O'Neill et al.*, 2002; *Dubovik et al.*, 2002; *Eck et al.*, 2003]. The treatment of aerosol size distributions and optical properties in aerosol retrieval algorithms is generally poor and varies from one algorithm to another. Inherent discrepancies are thus incurred between different aerosol products, which should be well understood and quantified before attributing the discrepancies to factors that are not readily verified such as cloud screening. The choice of aerosol models on retrieved AOT was deemed to be small (less than 10%) by *Geogdzhayev et al.* [2002] whose choice of aerosol models was not as diverse as those employed in the MODIS retrieval though. *Chylek et al.* [2003] found that the uncertainties in aerosol parameters such as refractive index and aerosol shape have large effects on the phase function at large scattering angles (greater than 100 degrees). As satellite aerosol retrievals are typically performed at such large scattering angles, the impact of aerosol model choice is expected to be significant.

[6] The objective of this study is to understand and quantify the uncertainties and discrepancies in the AOT and the α derived from the MODIS [*Tanré et al.*, 1997] and the AVHRR [*Mishchenko et al.*, 1999; *Geogdzhayev et al.*, 2002] with more focus on the possible effects of aerosol model difference. In a companion paper [*Jeong and Li*, 2005], other factors affecting the aerosol retrievals were also investigated. In section 2, the aerosol products used are briefly described. Section 3 presents the comparisons of the AOT derived from the MODIS and the AVHRR and investigations of their discrepancies. Similar studies but for α and its relation to aerosol effective radius are given in section 4. The summary and conclusive remarks are provided in section 5.

2. Data Sets

2.1. GACP/AVHRR Aerosol Product

[7] An AVHRR-based aerosol product generated under the Global Aerosol Climatology Project (GACP) [*Mishchenko et al.*, 1999; *Geogdzhayev et al.*, 2002] (updated at http://gacp.giss.nasa.gov/) is employed in this study (hereinafter the product will be referred to as GACP/AVHRR or simply AVHRR product). It contains the monthly mean aerosol AOT at 0.55 μm and α from July 1983 through September 2001 over oceans. The product resolution is 1×1 degree on an equal-angle grid. It was derived from clear-sky radiances from AVHRR channel 1 (nominal wavelength, $\lambda = 0.63$ μm) and channel 2 ($\lambda = 0.85$ μm) contained in the ISCCP DX data set [*Rossow and Schiffer*, 1999]. Note that the ISCCP radiance data were obtained following postlaunch calibration [*Brest et al.*, 1997]. Aerosol particles are assumed as homogeneous spheres whose optical properties are determined by the Lorenz-Mie theory. A modified power law size distribution was adopted with the aerosol refractive indices fixed as $m = 1.5 - 0.003i$. The shaping factor, which is the parameter that determines the shape of the modified power law size distribution, has a unique relationship with α and the effective radius of aerosols.

[8] There are many sources of errors inhibiting accurate aerosol retrievals [*Mishchenko et al.*, 1999]. Radiance calibration is one of the major uncertain factors [e.g., *Higurashi and Nakajima*, 1999; *Ignatov and Stowe*, 2002b] and can change the AOT by more than 40% [*Geogdzhayev et al.*, 2002]. Cloud screening could lead to very larger errors in AOT [*Ignatov and Nalli*, 2002; *Myhre et al.*, 2004]. More conservative cloud screening algorithms were applied by *Mishchenko et al.* [1999] and *Geogdzhayev et al.* [2002], in addition to the ISCCP cloud detection algorithm [*Rossow and Garder*, 1993]. The additional cloud screening aims to eliminate small cumulus clouds and optically thin cirrus clouds. However, the strict cloud masking may have an adverse impact of discarding useful aerosol signals by misclassifying them as clouds [*Husar et al.*, 1997; *Haywood et al.*, 2001]. For instance, an AOT threshold of 1 is used for the GACP/AVHRR product as a part of cloud screening, which will discard some cases with heavy aerosol loading. Other important error sources are the assumptions

about aerosols. *Mishchenko et al.* [1999] showed a use of fixed refractive index introduces systematic regional difference. *Geogdzhayev et al.* [2002] argued that the effect on the retrieved AOT of the choice of aerosol size distribution function would be less than 10%. *Mishchenko et al.* [2003] found that the spherical assumption can cause errors up to a factor of two for nonspherical particles like mineral dust. Other possible sources of error include uncertainties in boundary conditions (i.e., fixed wind speed and water-leaving radiance) and water vapor absorption at channel 2.

[9] In general, the accuracy of the α is known to be inversely proportional to the AOT [*Ignatov et al.*, 1998] and related to the spectral separation between the channels [*Ignatov and Stowe*, 2002b]. Yet, the accuracy of the α is lower than that of the AOT [*Ignatov and Stowe*, 2000]. *Geogdzhayev et al.* [2002] estimated that the retrieval accuracy in the α, when taking into account the calibration uncertainty, the choice of aerosol size distribution, and the selection of a fixed wind speed, was less than 0.4, 0.3 and 0.125, respectively. Use of a long-term climatology can suppress random-like errors especially those associated with radiometric noise and digitization [*Ignatov et al.*, 1998].

2.2. MODIS Aerosol Product

[10] The MODIS aerosol product was generated by different algorithms, depending on whether the surface was ocean [*Tanré et al.*, 1997] or land [*Kaufman et al.*, 1997]. Since the AVHRR aerosol product is retrieved over oceans only, aerosol products were selected from March 2000 through April 2001 when both AVHRR and MODIS aerosol products over ocean were available. The MODIS product is version 4 of the MOD08 data set with a spatial resolution of 1×1 degree. The product includes numerous parameters such as the AOT, α, the effective radius, the number of cloud condensation nuclei, the asymmetry factor, and the backscattering ratio. Employed in this study are AOT at 0.55 μm and α derived from the channels centered at 0.55 μm and 0.87 μm.

[11] The retrieval algorithm was originally documented by *Tanré et al.* [1997] and updated by *Levy et al.* [2003] and *Remer et al.* [2005]. It utilizes radiances observed at six bands (nominal wavelengths of 0.55, 0.66, 0.87, 1.24, 1.64, and 2.13 μm) at a spatial resolution of 500 m under clear-sky conditions determined by a dedicated cloud-masking algorithm [*Martins et al.*, 2002]. Aerosol particles are also assumed to be spherical as in the AVHRR AOT retrieval. However, the aerosol models employed in the MODIS algorithm are much more sophisticated than any prior algorithms. It adopted bimodal lognormal size distribution functions as suggested by measurements [*Whitby*, 1978; *Kaufman et al.*, 1994; *Kaufman and Holben*, 1996; *Dubovik et al.*, 2002] with 20 combinations of nine basic modes including four "fine" and five "coarse" modes. Each mode has a wavelength-dependent refractive index. Aerosol optical properties (single scattering albedo and phase function) were computed and stored as lookup tables (LUTs) for the 9 basic modes at various AOT values (0–2.0), 9 solar zenith angles, 16 satellite zenith angles, and 16 relative azimuth angles. Reflected radiances from the two lognormal size distributions are approximated by the weighted average of those for each individual distribution [*Wang and Gordon*, 1994]. A radiance measurement is matched to a weighted combination of computed radiances corresponding to the coarse and fine mode aerosols. The aerosol modes and weighting factors were selected based on the sum of square differences at six channels. Note that more than one aerosol model may be selected, depending if the radiance differences fall within the given margins of tolerance, rather than the minimum differences (L. Remer, private communication, 2004). The retrievals are averages of all the qualified values.

[12] The MODIS products have been validated over land [*Chu et al.*, 2002] and ocean [*Remer et al.*, 2002; *Levy et al.*, 2003] against AERONET data following a standardized procedure introduced by *Ichoku et al.* [2002]. *Remer et al.* [2002] showed AOT errors over ocean for nondust aerosols fall within the estimated accuracy of $\Delta\tau = \pm 0.03 \pm 0.05\tau$ [*Tanré et al.*, 1997] and the retrieved aerosol effective radius also agreed with that derived from AERONET to within ± 0.1 μm. For dust aerosols, *Levy et al.* [2003] found similar agreements in the AOT estimates but with a slight wavelength dependence, underestimation at 0.87 μm and overestimation at 0.47 μm and 0.55 μm. However, they reported a larger underestimation (20–100%) in the dust particle size, which was conjectured to stem from the spherical particle assumption. *Chu et al.* [2002] showed that the root mean square of errors (RMSE) of the MODIS AOT varied from 0.07 to 0.11 for inland regions, but increased up to 0.3 for coastal regions due to water color contamination. For the α, the MODIS values are correlated with AERONET values at a correlation coefficient of 0.50 for MODIS AOT greater than 0.20 at 0.66 μm.

3. Aerosol Optical Thickness (AOT)

3.1. Comparison of GACP/AVHRR and MODIS AOT

[13] Figure 1 shows the global distributions of the AOT from MODIS and AVHRR (upper panels) and their absolute and relative differences (lower panels). While the gross patterns of the AOT global distributions are similar to each other, their magnitudes are rather different, especially over regions affected by major aerosol regimes (e.g., off the west coast of Africa, the North Pacific Ocean, the North Atlantic Ocean, and spotty areas in the midlatitude Southern Hemispheric Oceans). The maps of absolute and relative differences reveal that the two AOTs agree with each other to within ± 0.2, with relative differences often exceeding 10% and sometimes reaching 100%. The largest discrepancies in AOT are found off the west coast of Africa by roughly up to 0.5. It is worth noting that larger discrepancies (>0.3) are mostly positive (i.e., MODIS AOT > AVHRR AOT) except for some patchy areas in the Southern Hemispheric Oceans (30–60°S).

[14] To gain further insight into these discrepancies, regional means of MODIS and AVHRR AOTs were compared for all the available months over regions influenced by various aerosol regimes. Figure 2 delineates all the rectangular regions under study together with the dominant aerosol types [cf. *Jeong and Li*, 2005]. The two mean AOTs are much better correlated, thanks to the averaging which eliminates/suppresses the random component of the discrepancies. However, there are significant regional differences,

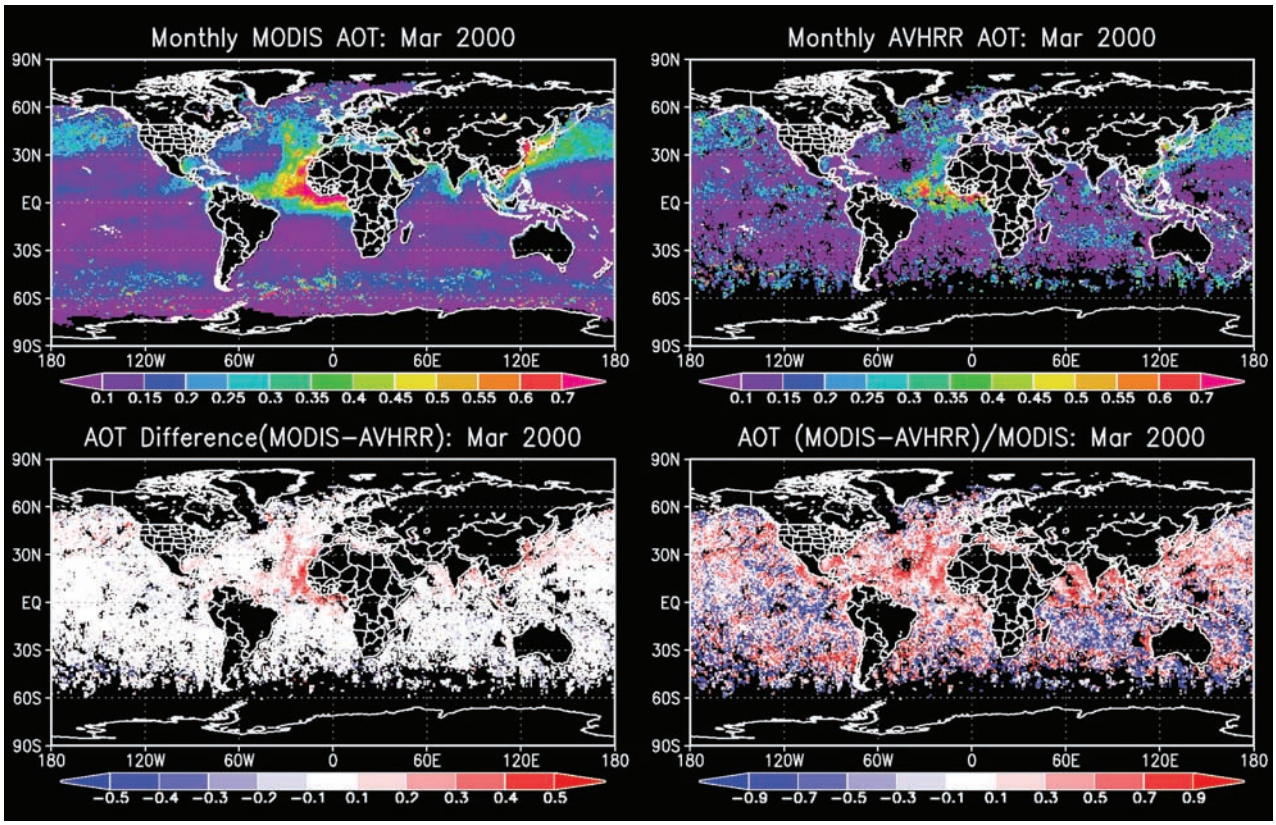

Figure 1. Monthly distribution of MODIS AOT, AVHRR AOT, their difference (MODIS minus AVHRR), and relative difference (March 2000).

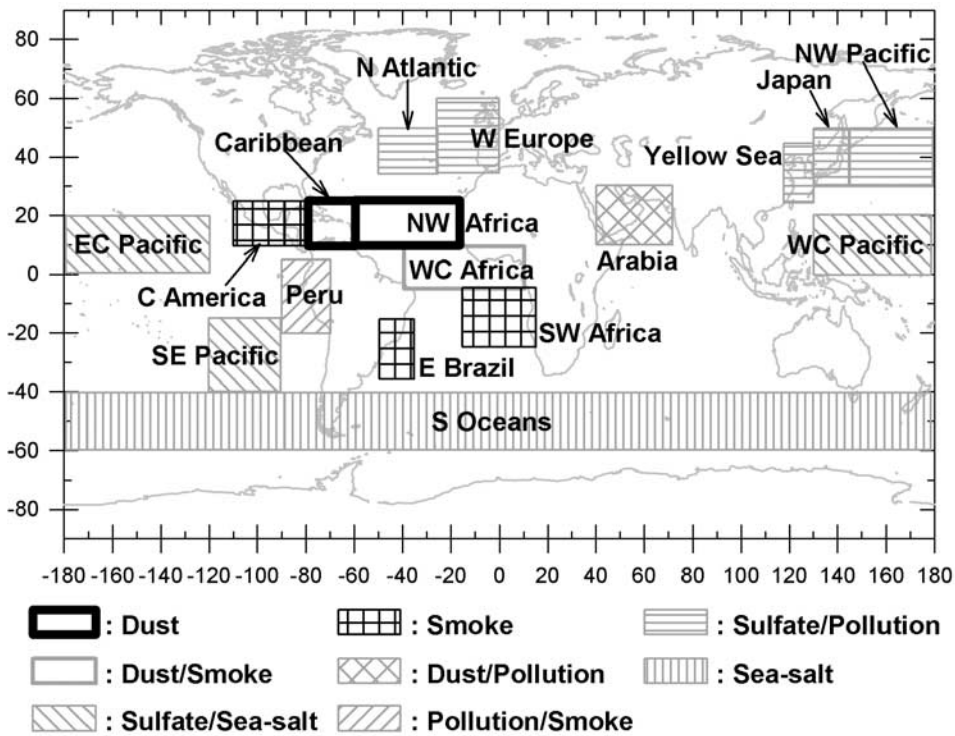

Figure 2. Aerosol regions over the oceans. Regions are defined as rectangles for which regional averages of AOT and Ångström exponent are calculated (see Figures 3 and 9). For some regions containing landmasses, averages were obtained only over water.

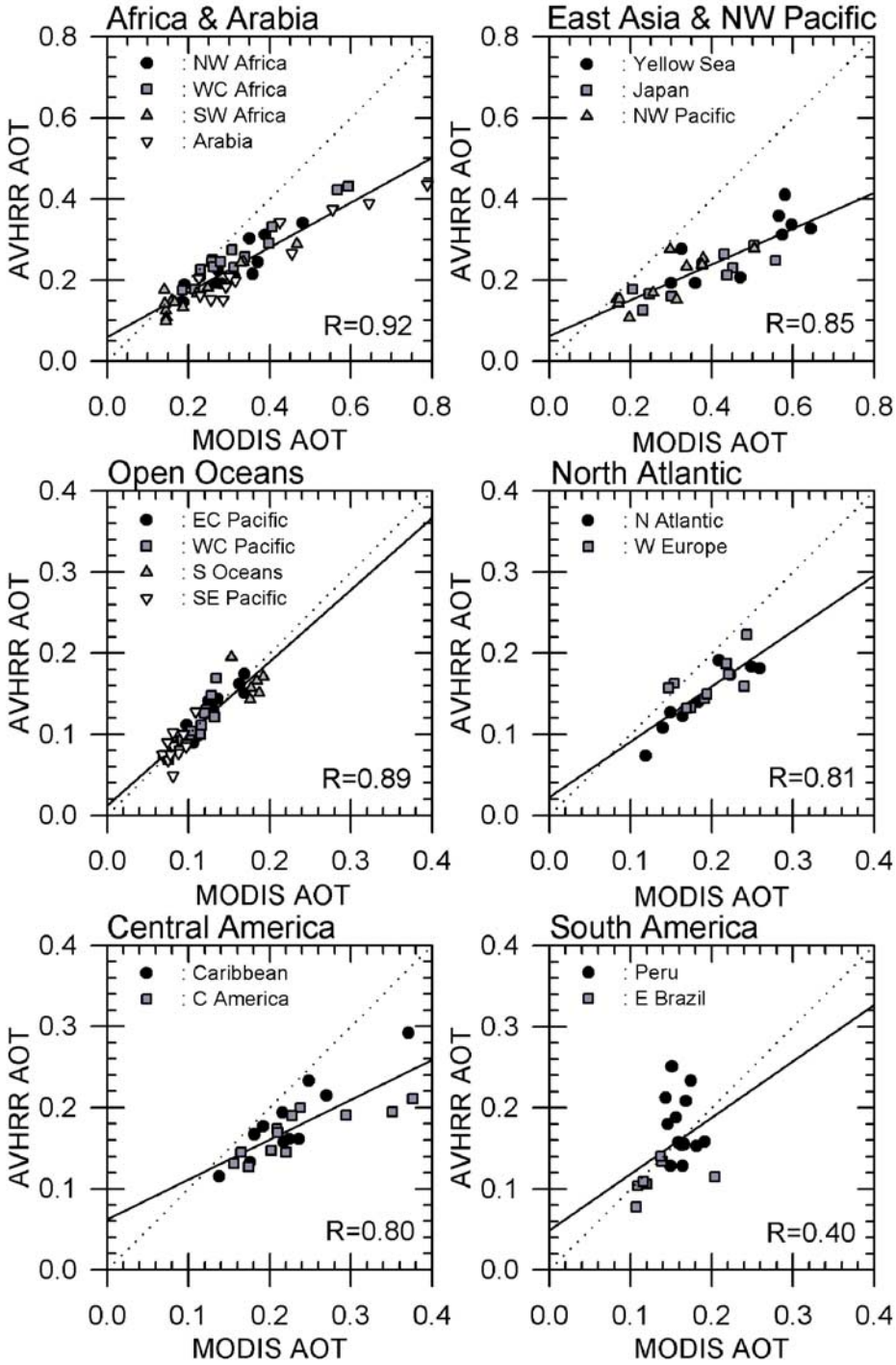

Figure 3. Comparison of colocated AVHRR and MODIS AOTs averaged over each region. Each symbol stands for areal average over the regions defined in Figure 2 for individual months. Black solid and dotted lines stand for linear fit curve and one-to-one line, respectively. Note that some regions are named in reference to the nearby continental locations, but they are all over oceans.

indicated by the slope of the regression line between the two sets of AOT. The slope is less than 1.0 (underestimation by AVHRR) for most regions of elevated aerosol loading by mineral dust, biomass/coal burning, and heavy pollution. Over the open oceans (EC/WC Pacific regions, SE Pacific, etc.), the two AOTs match well with each other. The low correlation found over the Central America and Peru regions likely results from the varying aerosol influences as discussed in the work of *Jeong and Li* [2005].

3.2. Factors Contributing to the AOT Discrepancies

[15] It is very important and challenging to unravel the physical causes for the systematic discrepancies. While errors in AOT retrievals are incurred by numerous factors,

Table 1. Aerosol Models Used in the Experiment for Testing the Impacts of Aerosol Model Selection[a]

MP Model		Small (Sx) and Large (Bx) Modes for BL Model				
ν	r_{eff}, μm	ID	m (λ = 0.47–086)[b]	r_g, μm	σ_g	r_{eff}, μm
2.5	3.63	S1	1.45–0.0035i	0.07	0.40	0.10
3.0	2.01	S2	1.45–0.0035i	0.06	0.60	0.15
3.5	0.86	S3	1.40–0.0020i	0.08	0.60	0.20
4.0	0.37	S4	1.40–0.0020i	0.10	0.60	0.25
4.5	0.21	B5	1.45–0.0035i	0.40	0.60	0.98
5.0	0.15	B6	1.45–0.0035i	0.60	0.60	1.48
		B7	1.45–0.0035i	0.80	0.60	1.98
		B8	1.53–0.0030i (0.47 μm)	0.60	0.60	1.48
			1.53–0.0010i (0.55 μm)			
			1.53–0.0000i (0.66 μm)			
			1.53–0.0000i (0.86 μm)			
		B9	1.53–0.0030i (0.47 μm)	0.50	0.80	2.50
			1.53–0.0010i (0.55 μm)			
			1.53–0.0000i (0.66 μm)			
			1.53–0.0000i (0.86 μm)			

[a]As for the MP models, 26 shaping factor (ν) values, ranging from 2.5 through 5.0 with an interval of 0.1, were used in this study, but only six cases are shown in the table. Detailed description for BL models that are used by the MODIS aerosol retrieval algorithm can be found in the work of *Levy et al.* [2003, Tables 1a and 1b].

[b]Here m denotes refractive indices. Note that refractive indices for MP models are fixed as m = 1.5–0.003i.

cloud screening was often blamed for any large discrepancies [*Myhre et al.*, 2004]. We agree that cloud screening contributes significantly to the discrepancies as shown in Figure 1. Clouds affect the performance of aerosol retrievals in three ways [e.g., *Husar et al.*, 1997; *Haywood et al.*, 2001; *Jeong and Li*, 2005]: (1) through cloud contamination, (2) misclassification of aerosols as clouds, and (3) bias in aerosol sampling due to presence of clouds (i.e., no retrieval for cloudy pixels). The first effect leads to overestimation of the AOT, the second to underestimation of the AOT, and the third to either overestimation or underestimation of the AOT (thus produces random-like errors). It is more likely that misclassification of aerosols as clouds underestimates the AOT for instances of high aerosol loading, while cloud contamination results in AOT overestimation under any instance of aerosol loading. One may thus conjecture that the discrepancies shown in Figure 3 are caused by misclassification of clouds and aerosols in the AVHRR product or by cloud contamination in the MODIS product. Unfortunately, this inference cannot be tested with the data available for this investigation, which would require analysis of individual scenes for better discrimination between cloud and heavy aerosol episodes.

[16] One must also bear in mind that other factors may be as important as cloud in causing the discrepancies. Use of different types of aerosol models can be a major source of discrepancy. The aerosol models are differentiated by aerosol particle size distribution and refractive index. The following model simulations offer insights into the impact of the aerosol size distribution and refractive indices defining the different aerosol models used by the MODIS and the AVHRR retrievals. The AVHRR retrieval algorithm adopts a modified power law size distribution (hereinafter referred to as the MP model) and a fixed refractive index. The MODIS algorithm employs a bimodal lognormal size distribution (hereinafter referred to as BL models). The two functions of aerosol size distribution have often been employed in aerosol retrievals from space [*Stowe et al.*, 1997; *Mishchenko et al.*, 1999; *Higurashi and Nakajima*, 1999; *Tanré et al.*, 1997]. They are given as follows:

[17] Modified power law:

$$n(r) = \begin{cases} C, & r \le r_1 \\ C \cdot (r/r_1)^{-\nu}, & r_1 < r \le r_2 \\ 0, & r > r_2. \end{cases} \quad (1)$$

where $r_1 = 0.1$ μm, $r_2 = 10.0$ μm, and the shaping factor, $\nu \in [2.5, 5.0]$. C is a normalization constant chosen to satisfy the condition that

$$\int_0^\infty n(r)dr = 1.$$

[18] Bimodal lognormal:

$$n(r) = \frac{dN(r)}{dr} = \sum_{j=1}^{2} \frac{dN_j(r)}{dr}, \quad (2)$$

$$\frac{dN_j(r)}{dr} = \frac{N_j}{(2\pi)^{1/2}\sigma 2.3r} \exp\left\{ -\frac{\left(\log r - \log r_{m,j}\right)^2}{2\sigma^2} \right\},$$

where N is the density number, r_m is median radius, and $\sigma^2 = \langle(\log\ r\ -\ \log\ r_m)^2\rangle$.

[19] The MODIS BL models are combinations of two individual lognormal size distributions with one of four small modes (denoted as S1–S4 in Table 1) and another out of five large modes (B5–B9). The refractive index for each model is also listed in the table. In addition to the choice of 20 combinations of small and large modes, the MODIS aerosol model also varies with a weighting factor between the small and large modes. In this study, 220 (=20 × 11) cases are used by changing the weighting factor from 0 to 1 with an interval of 0.1. Likewise, simulations with the MP model assumed 26 values for the exponent of the size distribution (i.e., the shaping factor) ranging from 2.5 through 5.0 with an interval of 0.1. Mie calculations were first conducted to generate the optical properties of each model aerosol and these were then fed into the SBDART radiative transfer model [*Ricchiazzi et al.*, 1998] to compute reflectance at the top of the atmosphere. The computational burden was lowered considerably by adopting an approximation proposed by *Wang and Gordon* [1994] that was also employed in the MODIS algorithm [*Tanré et al.*, 1997]. The approximation treats radiance due to multiple scattering from two lognormal modes as a weighted average of radiances from each individual mode for the same optical thickness.

[20] The ocean surface boundary condition was based on *Cox and Munk* [1954] with the wind speed set to 7 m/s, as was employed by both MODIS and AVHRR algorithms [*Geogdzhayev et al.*, 2002; *Levy et al.*, 2003]. The standard midlatitude summer atmosphere [*McClatchey et al.*, 1972] was assumed, together with exponentially decreasing aerosol number density with increasing altitude as was provided by 5S [*Tanré et al.*, 1990]. Note that atmospheric profiles have little influence on the retrievals [*Mishchenko et al.*,

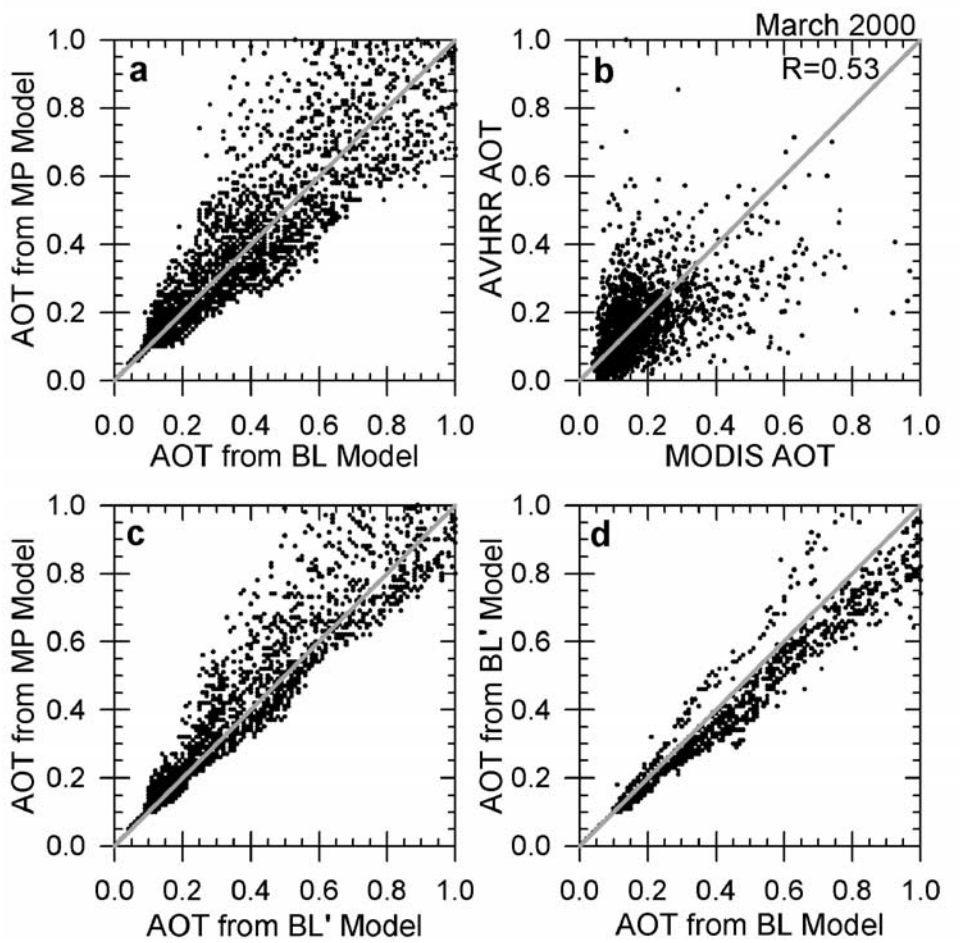

Figure 4. (a) Scatterplot of AOT from MP models versus that from BL models. (b) Scatterplot of observed AOT from MODIS and AVHRR (global; March 2000). (c) The same as Figure 4a but refractive index for BL models were replaced by a single fixed value (i.e., m = 1.5–0.003i) as used in the MP models, which are referred to as BL′ models. (d) Analogous to Figures 4a and 4c except for BL′ versus BL models. Gray solid line is the one-to-one line.

1999]. Radiances were simulated for all possible satellite-Sun geometries with the scattering angle varying from 90 to 180 degrees. To avoid Sun glint, calculations for which the zenith angle of the reflected light is within a cone of 40 degrees from the direction of specular reflection for a flat surface were excluded as was done in both MODIS and AVHRR retrievals [*Mishchenko et al.*, 1999; *Tanré et al.*, 1997; *Levy et al.*, 2003]. The AOT at 0.55 μm was allowed to change from 0.01 to 1.0. The AOTs associated with the MP models were matched with those from the BL models according to reflectances computed by the two models at the two nominal AVHRR wavelengths (0.63 μm and 0.83 μm). The margin of match in reflectance was set to 1×10^{-4} which is a very high accuracy compared to the uncertainties in ISCCP channel 1 reflectance data (±0.01–0.02) [*Brest et al.*, 1997].

[21] The overall comparison of matched AOTs simulated by the models is shown in Figure 4a. They exhibit very large discrepancies by up to a factor of two. This suggests that the selection of a particular aerosol model is an important factor influencing the retrieval of the AOT. However, its range of effect is still smaller than that of the observed differences between the MODIS and the AVHRR as is shown in Figure 4b. Since the two types of aerosol models differ in both size distribution and refractive index, a further attempt is made to separate the impact of the two factors by setting the refractive index of the BL models to the same value as the MP models (i.e., m = 1.5–0.003i) but retaining the original size parameters. They are referred to as BL′ models. Figure 4c presents the same scatterplot as

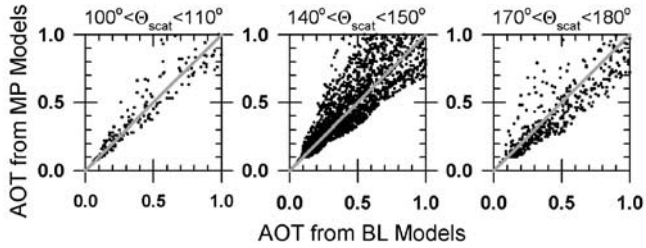

Figure 5. The same as Figure 4a, but scatterplots are presented separately for the scattering angles, 100–110°, 140–150°, and 170–180°.

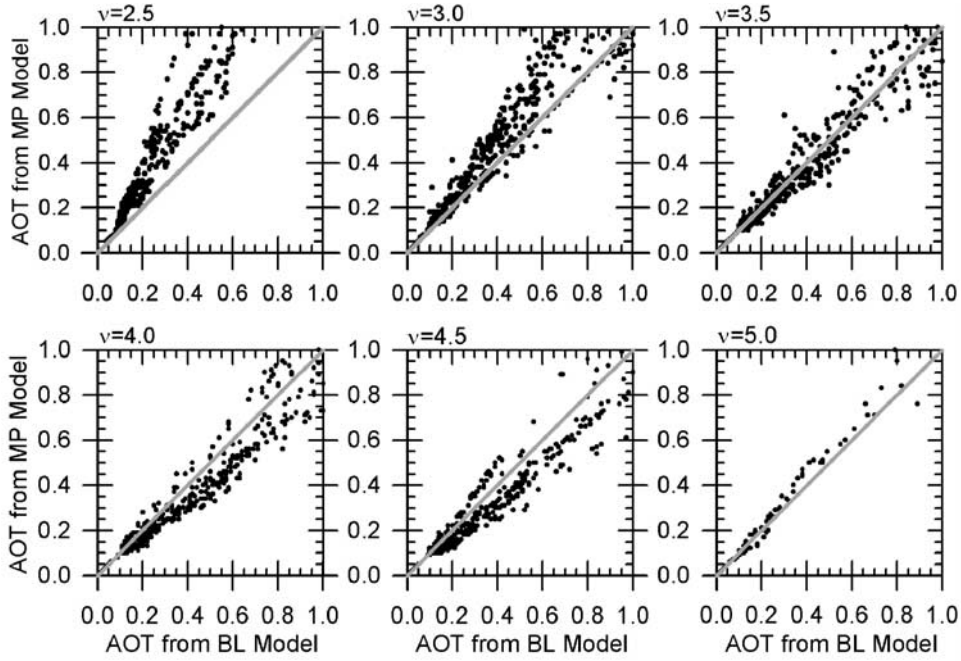

Figure 6. Same as Figure 4a, but the scatter diagrams are plotted according to the exponent (i.e., the shaping factor) of the MP models.

in Figure 4a but compares the AOTs retrieved with the MP and BL′ models. The scattering is almost as large as in Figure 4a but shows more systematic differences with the AOT from the MP model larger than that from the BL′ model. This implies that the difference in size distribution functions contributes to the substantial discrepancies between the MODIS and the AVHRR AOTs. This finding underlines the importance of selecting the most appropriate aerosol size distribution function in the retrieval of the AOT. The biased distribution in Figure 4c and the more symmetric distribution in Figure 4a suggest that the refractive index has an opposite effect, which is reinforced by a comparison of the AOTs retrieved from the BL versus BL′ models (Figure 4d). Since the two models have the same size distribution but different refractive indices, the resulting differences reflect the sole effect of refractive index. The absolute difference is less than 0.2 for almost all the cases, but increases with increasing AOT within a difference range of $\pm 0.2\tau$. It should be noted that our simulation result indicates the bulk range of potential errors incurred by differences between the two aerosol models, implying that for fixed

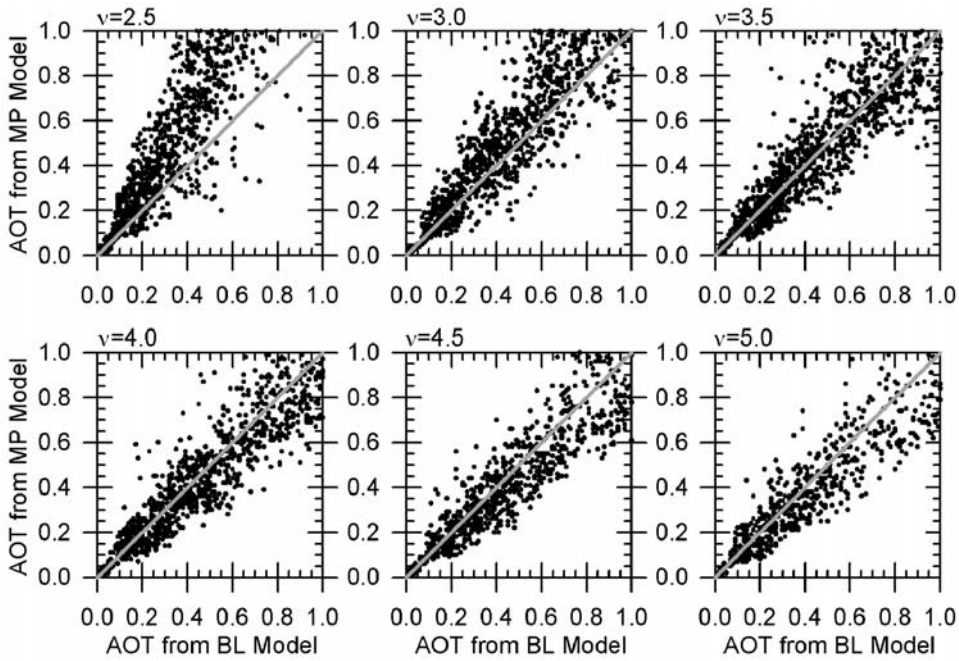

Figure 7. The same as Figure 6, but with a permitted reflectance error of 10^{-2}.

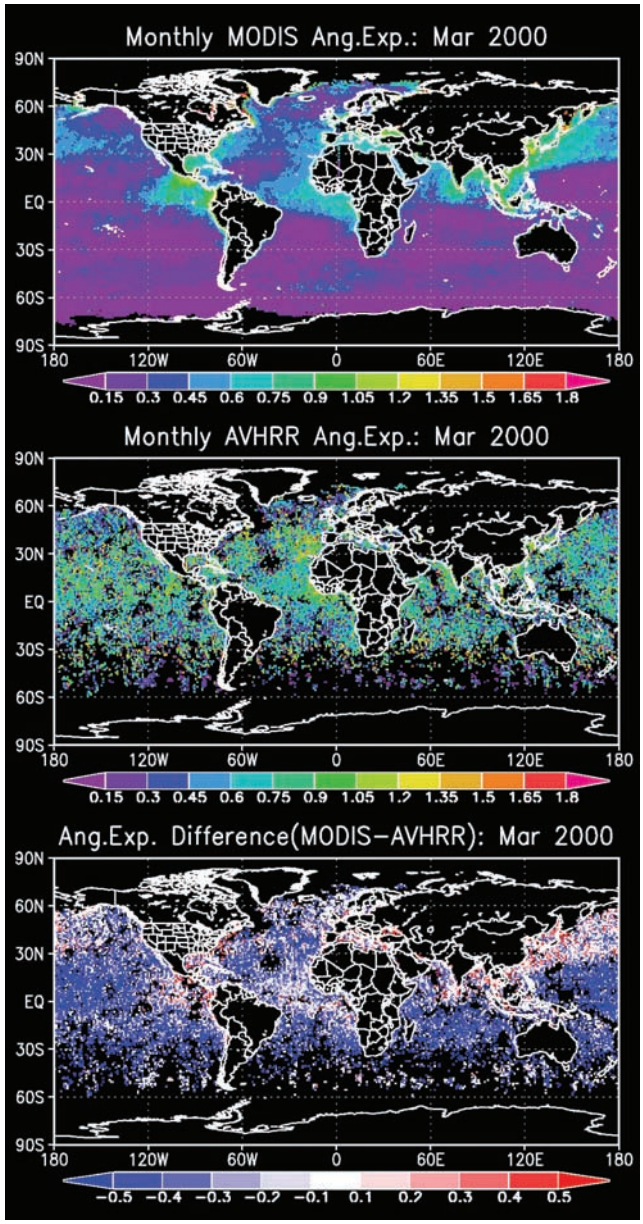

Figure 8. Monthly distributions (March 2000) of (top) MODIS and (middle) AVHRR Ångström exponent and (bottom) their difference (MODIS minus AVHRR).

radiances, retrieval of AOT is very sensitive to the selection of aerosol models.

[22] The comparisons shown in Figure 4 suggest that the aerosol size distribution is one of key factors responsible for the large random discrepancies in the AOT retrievals from the MODIS and the AVHRR, while both the size distribution and refractive index contribute to the systematic differences. Another hidden factor that is linked to the aerosol model difference is the scattering angle. Different aerosol models have different phase functions and the differences in phase function vary with the scattering angle. Figure 5 shows the comparisons of the AOT retrieved from the BL and MP models for three ranges of potential scattering angles: 100–110, 140–150, and 170–180 degrees. There are large differences of about the same sign and magnitude as seen in Figure 4a for both low and high angles. Note that the dominant scattering angle for both the AVHRR and the MODIS is centered around 140–150 degrees.

[23] In Figure 6, all the data used in Figure 4a were grouped according to the exponent (i.e., the shaping factor; ν) of the MP model. The discrepancies in AOT between the MODIS and AVHRR products show a clear dependence on the shaping factor in the AVHRR algorithm. For example, for a small shaping factor (e.g., $\nu = 2.5$; large particles), the AVHRR AOT could to be larger than the MODIS AOT by up to a factor of two. However, for a larger shaping factor (e.g., $\nu = 5.0$; small particles), the two agree well with each other. Assuming ν ranged from 2.5 to 3.0 for sea salt, 3.0 to 3.5 for dust, 4.0 to 4.5 for biomass burning, and 4.5 to 5.0 for sulfate/pollution [cf. *Mishchenko et al.*, 1999, Figure 7], we may make some interesting inferences with reference to Figure 3. First, for the dust regimes such as NW Africa and Arabia, the AVHRR AOT (i.e., AOT from MP model) is expected to be higher than the MODIS AOT (AOT from BL model) according to our simulation, while the observations show an opposite result. Second, for east Asia and NW Pacific regions where pollution is known to be dominant, our simulation suggests the MODIS AOT should be slightly higher or about the same as the AVHRR AOT. There is a weak agreement with the observations. Third, for open ocean regions such as EC Pacific and S Oceans where sea salt is presumably dominant, the observations reveal good agreements between the two AOTs, contrary to the simulation result suggesting higher AVHRR AOT than the MODIS AOT. We may thus infer that the difference in cloud screening might be a more significant factor than the aerosol model difference. It is almost certain that the lower AVHRR AOT values over heavy dust regions result from the ceiling of the AVHRR AOT product, which most likely exceeds the effects of aerosol model difference. For east Asia and NW Pacific, both effects render higher MODIS AOT than the AVHRR AOT. Good agreements in the open oceans may be explained by the compensation of the two offsetting effects.

[24] Another important factor is the radiometric uncertainty in AVHRR measurements. To evaluate this effect, we performed the same simulation but permitting larger reflectance errors of 10^{-2}, which corresponds to the level of the radiometric uncertainties of ISCCP data [*Brest et al.*, 1997]. The results are presented in Figure 7. For each shaping factor group, the ranges of discrepancies are larger than those found in Figure 6, as one would expect. However, the overall ranges of the AOT discrepancies remain virtually the same, if the points from all the panels were put together. We may, therefore, conclude that the radiometric uncertainties in the AVHRR affect more significantly the selection of aerosol models (i.e., size or α) than the retrieval of AOT. It is thus unlikely to explain the systematic differences between the MODIS and GACP/AVHRR AOTs, unless there were biases due to radiometric calibration that are much larger than those reported by *Brest et al.* [1997].

4. Ångström Exponent (α)

4.1. Evaluation and Comparison of GACP/AVHRR and MODIS α

[25] The global distributions of the Ångström exponent (α) derived from MODIS and AVHRR shows more

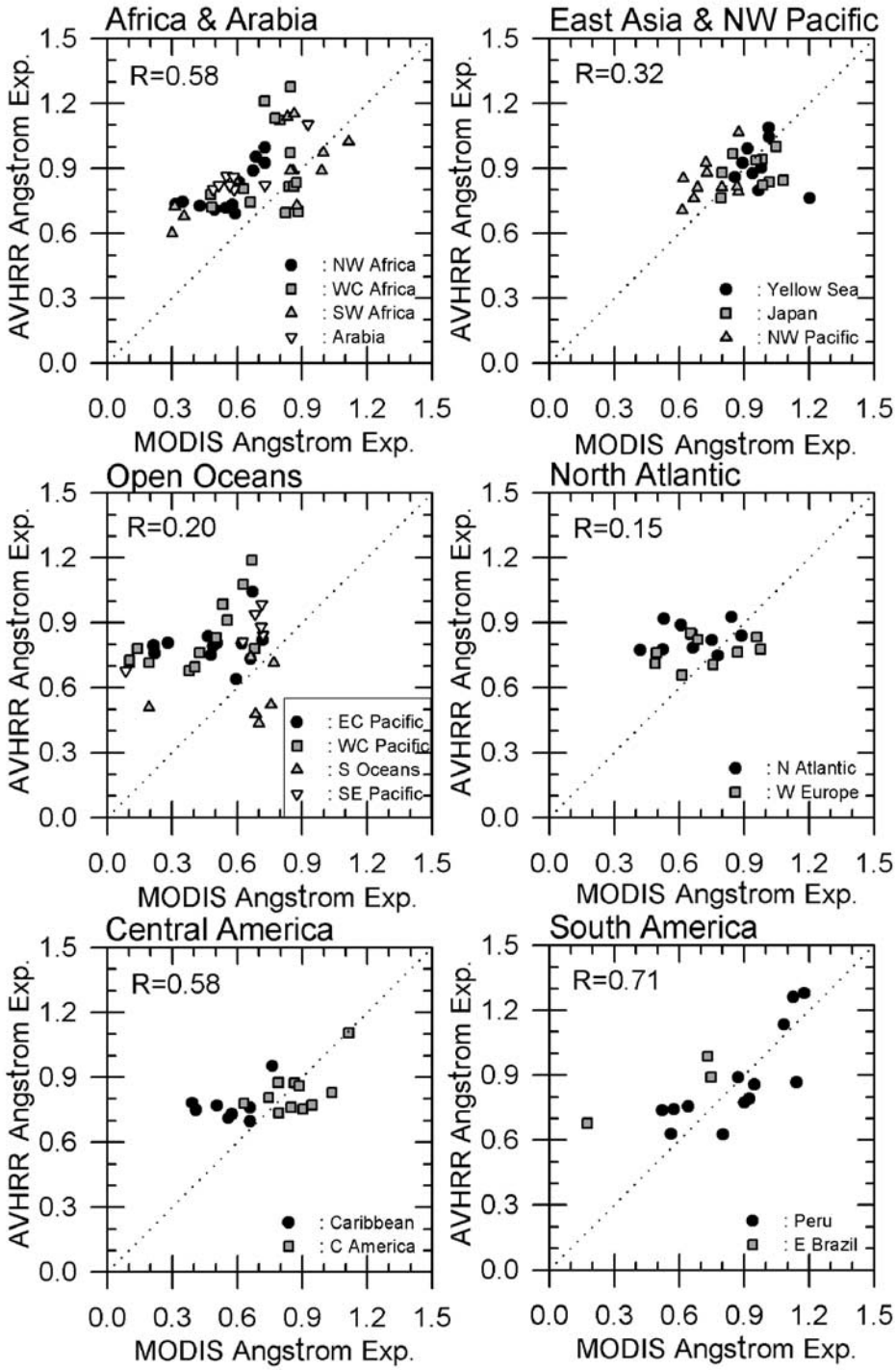

Figure 9. Comparison of colocated AVHRR and MODIS Ångström exponent averaged over each region. Dotted lines stand for the one-to-one line.

substantially different features than those of the AOT (Figure 8). First, individual monthly α from AVHRR (α_{AVHRR}) is much more noisier than that from MODIS (α_{MODIS}). The α_{MODIS} is large near the coasts, and decreases toward the ocean interior. This trend of variation is far less clear for α_{AVHRR} due to its noisy distribution pattern. In a similar manner for the regional characteristics, α_{MODIS} is smaller (0.4–0.6) in NW Africa and larger ($\sim$1.2) in SW Africa. For α_{AVHRR}, the general trend is somewhat similar but much less obvious. As such, the difference ($\Delta\alpha_{MA} = \alpha_{MODIS} - \alpha_{AVHRR}$) map (bottom panel in Figure 8) shows structured patterns: large positive $\Delta\alpha_{MA}$ along the coastlines and regions dominated by smaller particles (e.g., NW Pacific, and C America), large negative $\Delta\alpha_{MA}$ over the open oceans where the AOT is small (<0.2), and small $|\Delta\alpha_{MA}|$ over NW/WC Africa, where the AOT is large. A large uncertainty exists in the estimates of α for small AOT

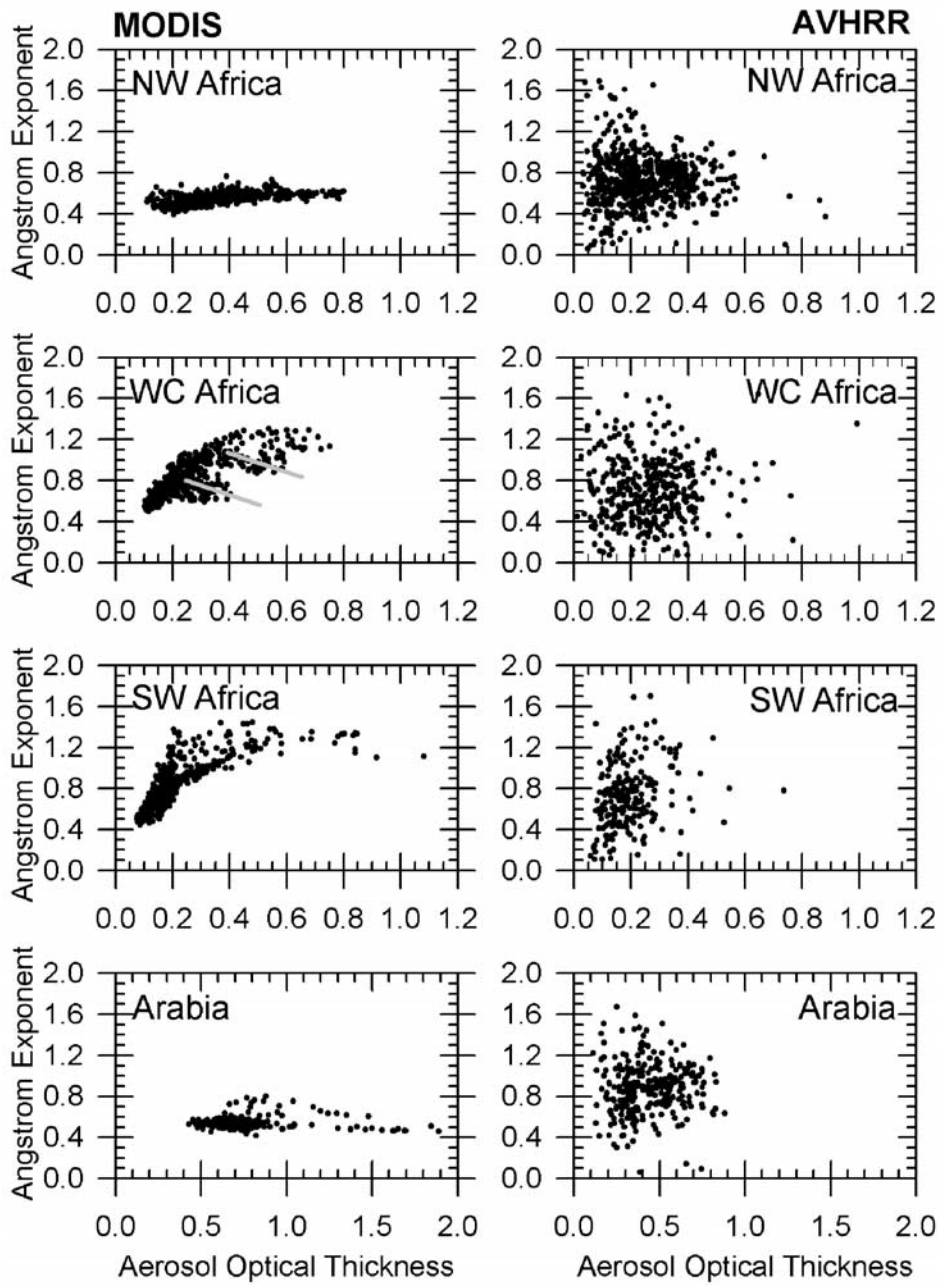

Figure 10. Scatterplots of Ångström exponent versus AOT. Left panels are based on MODIS data, while the right panels are from AVHRR data for the same period (July 2000). Gray lines provided in the WC Africa region for MODIS indicate possible signals from dusts coexisting with biomass burning aerosols in this region.

(<0.2) [*Ignatov et al.*, 1998; *Higurashi and Nakajima*, 1999], which may explain the large discrepancies found over open oceans.

[26] After averaging over a long period (about 13 years), the distribution of α_{AVHRR} [cf. *Jeong and Li*, 2005, Figure 1] are much more similar to α_{MODIS}, but the magnitudes and dynamic ranges of the two still differ significantly. Likewise, the regional averages of α_{AVHRR} are better correlated with those of α_{MODIS}, although the correlation coefficients are not high, as is shown in Figure 9 for the 17 regions defined in Figure 2. This is in contrast to the generally high correlations between AOTs derived from MODIS and AVHRR over the same regions as is shown in Figure 3. In general, α_{AVHRR} shows a considerably narrower dynamic range of variation than that of α_{MODIS}. Regions of low correlation in α correspond to low AOT.

[27] The quality of the satellite-based estimates of α can be evaluated by plotting it as a function of the AOT for the four aerosol regions. As is shown by *Eck et al.* [1999] using AERONET measurements, this kind of plot shows unique relationships for different types of aerosols. For instance, for biomass burning aerosols, α should increase with AOT. As the AOT increases, the proportion of smoke aerosols grows larger. Since smoke aerosol particle size is small, it leads to

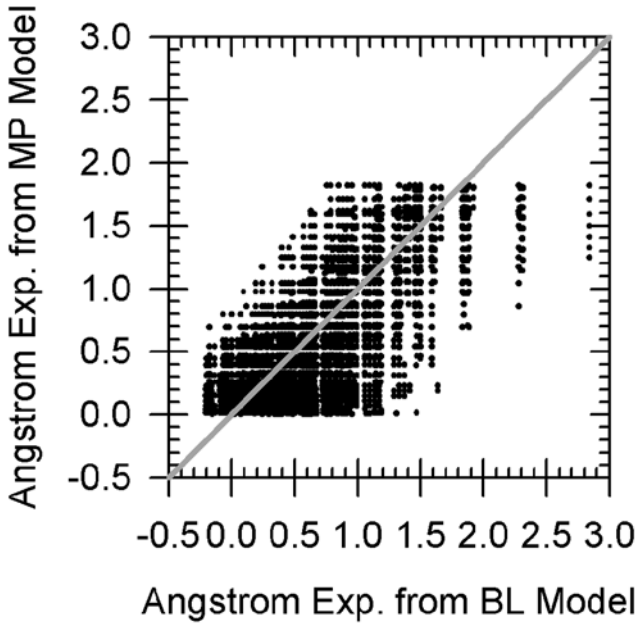

Figure 11. Same as Figure 4a except for Ångström exponent.

larger α. The expected positive correlation between the AOT and α, or negative correlation between the AOT and the particle size, is clearly seen in Figure 10 over the west central and South African regions. Similar results were obtained by *Reid et al.* [1999] from in situ airborne measurements during the Smoke/Sulfates, Clouds and Radiation-Brazil campaign [*Kaufman et al.*, 1998]. By the same token, one would expect to see a good correlation, but of opposite sign, between α and the AOT for dust aerosols since dust particles are larger in size than the background aerosols. Such a trend is not observed over the ocean off NW Africa and the Arabian Sea, where dust plays a dominant role; α tends to be constant around 0.4–0.6, although the data points are tightly clustered together. This may be explained by the fact that given the distance of these bodies of water from the source of dust generation, the gigantic dust particles lifted by strong dust storms have time to wash out of the atmosphere due to gravitational settling. As a result, the size of transported dusts is rather constant so that α is invariant with the AOT. This invariance in dust particle size has been reported by *Maring et al.* [2003] in their aircraft measurements of dust particles over the Canary Islands and Puerto Rico. It is interesting to note that the signals of biomass burning, dust and their mixture from MODIS data coexist over the WC African region. In contrast, similar plots for AVHRR-retrieved AOT and α are all widely scattered without showing any of the above features.

[28] The large uncertainties in the estimates of α_{AVHRR} warrants much caution when using it to address climate issues such as aerosol indirect effects. It is our belief that the monthly values of α_{AVHRR} contain so much uncertainty that it is of limited utility for climate studies, while the long-term and/or regional means contain certain useful information. The uncertainty may originate from calibration errors at the two channels of AVHRR and/or errors related to the retrieval algorithm. As pointed out in other studies [*Ignatov et al.*, 1998; *Higurashi and Nakajima*, 1999], α is very sensitive to errors in the spectral AOTs, especially for small AOT values. Relative to α_{MODIS}, α_{AVHRR} is noisy even for higher AOT (>0.4). In the following discussions, we investigate the impact of various factors on estimates of α, especially the aerosol size distribution, optical properties, and selection of wavelength pairs from which α is derived.

4.2. Factors Influencing α and its Discrepancies Between MODIS and GACP/AVHRR

[29] To investigate the impact of aerosol model differences between MODIS and AVHRR aerosol retrieval algorithms, α is calculated based on the BL and MP models, respectively, following the work described in section 3.2. Differences in the pair of channels used to derive α are taken into account so that α from the MP models (α_{MP}) is derived from the AOTs at 0.63 μm and 0.83 μm while α from the BL models (α_{BL}) is derived from the AOTs at 0.55 μm and 0.87 μm. A comparison of α_{BL} as a function of α_{MP} is plotted in Figure 11. The discrepancies between α_{MP} and α_{BL} are fairly large (~0.5), almost comparable to the observed differences, suggesting that the impact of the aerosol model differences could potentially explain a good portion of the observed discrepancies in magnitude but not necessarily in its spatial distribution pattern.

[30] Since the observed discrepancies stem partially from the use of different wavelength pairs, the effect of wavelength selection is studied first. Typically, α is computed by

$$\alpha = -\ln\left(\tau^a_{\lambda 1}/\tau^a_{\lambda 2}\right)/\ln(\lambda_1/\lambda_2), \tag{3}$$

or more generally,

$$\alpha = -\frac{d\ln C_{ext,\lambda}}{d\ln\lambda}, \tag{4}$$

where $C_{ext,\lambda}$ is the spectral extinction cross section. The α can be computed from the AOT (τ^a_λ) measured at two wavelengths or by means of regression of the AOTs measured at several wavelengths. The wavelengths chosen do not include the absorption bands due to ozone, water vapor and other absorbing gases. Also, whether the selected wavelengths can resolve the particle size of interest is taken into consideration. Measurements at different spectral regions have been employed including the visible (0.4–0.7 μm), near-infrared (around 0.87 μm, excluding water vapor absorption bands), and/or UV-A (0.34–0.38 μm) [*Iqbal*, 1983; *Holben et al.*, 1998; *Kinne et al.*, 2001]. Here, four pairs of wavelengths are considered: 0.66–0.87 μm, 0.55–0.87 μm, 0.47–0.66 μm, and 0.47–0.55 μm, which comprise the nominal wavelengths of the MODIS and AVHRR channels. The following pairs are actually used to derive α: 0.55–0.87 μm for MODIS ocean, 0.47–0.66 μm for MODIS land, and 0.66–0.87 μm for AVHRR. In addition, α is also derived from regression of the AOTs at all four wavelengths (i.e., 0.47, 0.55, 0.66, and 0.87 μm). Since α derived from the MP model is not sensitive to the selection of wavelength, the study is limited to BL models.

[31] Figure 12 shows the comparisons of the Ångström exponents computed from the four wavelength pairs. The Ångström exponents simulated for the MODIS ocean algo-

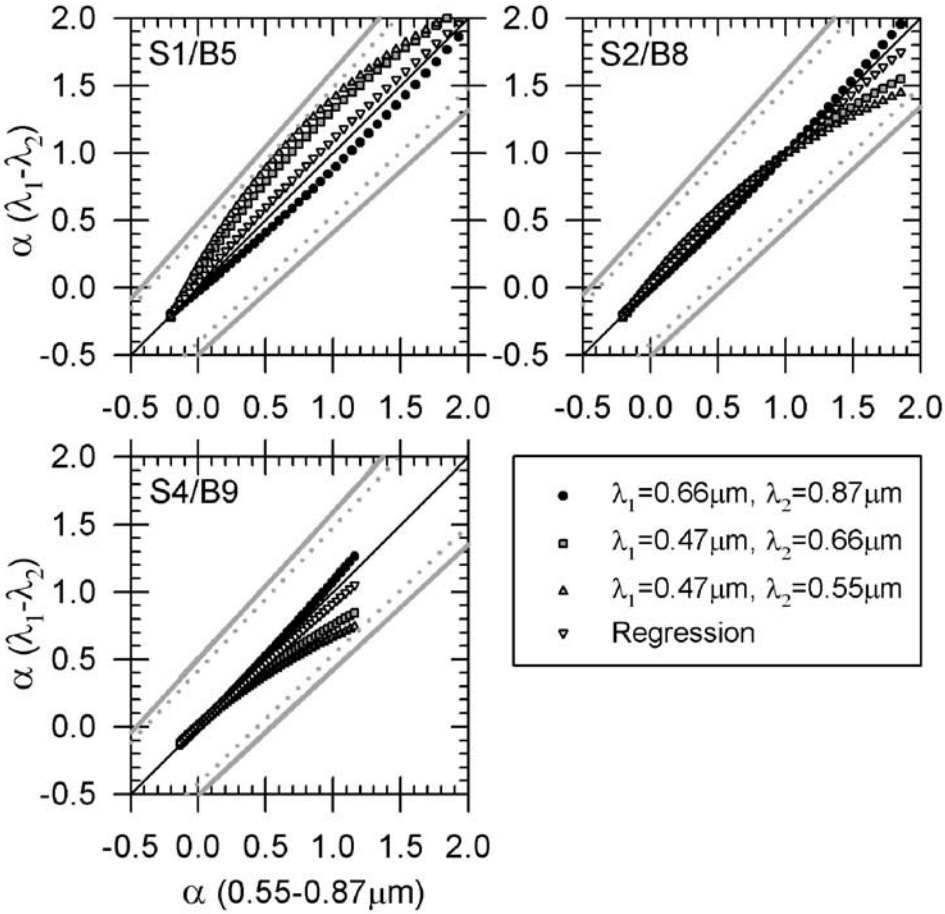

Figure 12. Influence of wavelength selection on Ångström exponent for three different BL models (S2/B8, S1/B5, and S4/B9). Ångström exponent was calculated for several combinations of two wavelengths from equation (3). Regression solution is calculated via linear regression for the four wavelengths (0.47, 0.55, 0.66, and 0.87 μm) in log τ −log λ space. Thick gray solid lines represent marginal errors of Ångström exponent due to spectral AOT errors of ±0.05τ ±0.03 for the wavelength pair of 0.55 and 0.87 μm, while the gray dotted lines are those for regression solution from AOTs at the four wavelengths. Thin solid line is the one-to-one line.

rithm is plotted as *X* axis, and the remainders are shown in *Y* axis, one of which is for AVHRR simulation. It is seen that the discrepancies resulting solely from the wavelength differences between MODIS and AVHRR are rather insignificant (<0.1). However, possible errors in spectral radiance measurements and an inconsistent estimation of the spectral AOT can cause much larger differences, especially when the signs of the errors for different wavelengths are opposite to each other [*Ignatov et al.*, 1998; *Ignatov and Stowe*, 2000]. The best accuracy in current satellite-based AOT estimations is expected to be ±0.05τ ±0.03 (for MODIS; *Remer et al.* [2002]). As shown in Figure 12, such AOT errors can cause very large errors in α (up to ±0.5). In this sense, a regression solution of α using several wavelengths, if available, is an effective means of suppressing this kind of error. As is also shown in the Figure 12, α from the regression is less vulnerable to errors in individual channels.

[32] A major utility of the Ångström exponent is to infer basic information about aerosol particle size [*Holben et al.*, 1991; *O'Neill and Royer*, 1993; *Nakajima and Higurashi*, 1998; *Eck et al.*, 1999]. While qualitative information pertaining to aerosol particle size may be readily gained from α, quantitative estimation of the aerosol effective radius (r_{eff}) from α would be much more cumbersome due in part to the strong dependence of the relationship between r_{eff} and α on the selection of aerosol size distribution, as is shown in Figure 13. The relationships were obtained for various BL and MP models with fixed complex refractive index (m = 1.5–0.003i). The BL models are from 20 different combinations of small and large modes, and one MP model with varying shaping factor. α is calculated for the wavelength pair of 0.55–0.87 μm. It is seen that corresponding to a fixed value of α is a wide range of r_{eff} that depends on the aerosol size distribution. The family of BL curves differs considerably among themselves, and even more from the MP curve, especially for low values of α (say, α < 0.5). This implies that for large particles α can be related to drastically different values of r_{eff} simply by assuming different size distribution models, posing a major difficulty in obtaining aerosol particle size.

[33] In addition to aerosol size distributions, aerosol absorption is another major factor influencing the retrieval of the AOT. Since the two types of aerosol models employed in MODIS and AVHRR retrievals differ in refractive index as well as in the size distribution, the resulting differences in single-scattering albedo (SSA) also contribute to discrepancies in AOT retrievals. Figure 14 shows a comparison of the SSA computed from the two aerosol models that generate the same reflectances. The SSA from the MP model is dependent only on aerosol size (shaping factor or α) when the refractive index is fixed so that significant errors are expected for large nonabsorbing (at visible and near-infrared) aerosols (e.g., dust), and for small absorbing aerosols (e.g., smoke) [*Mishchenko et al.*, 2003]. The contradicting finding that the AVHRR AOT is significantly lower than that from MODIS for the Saharan region implies that the AOT for dust is severely underestimated by the AVHRR [*Haywood et al.*, 2001]. This is most likely caused by misclassification of aerosol scenes as clouds. While, in general, good AOT retrieval accuracies were reported for nondust aerosols retrieved from MODIS [*Remer et al.*, 2002], the AOT underestimation for some smoke events was attributed to slightly higher SSA for smoke assumed in MODIS algorithm [*Ichoku et al.*, 2003].

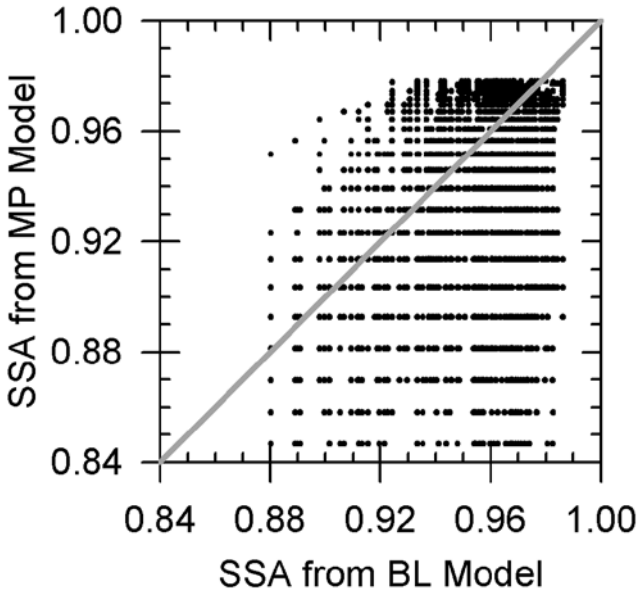

Figure 14. Same as Figure 4a except for single scattering albedo (SSA).

5. Summary and Conclusion

[34] In light of large discrepancies among various satellite-based global aerosol products, two prominent monthly global aerosol products retrieved from GACP/AVHRR [*Mishchenko et al.*, 1999] and MODIS [*Tanré et al.*, 1997] measurements are compared and factors leading to their discrepancies are explored. Comparisons of the monthly aerosol optical thickness (AOT) at 1 × 1 degree resolution showed substantial scattering and moderate systematic differences. However, their regional means (also long-term means) are much better correlated with the general tendency that the AVHRR values are smaller than the MODIS values, especially for heavy aerosol loadings. Difference in the cloud screening is likely a factor [*Myhre et al.*, 2004], but other factors can also come into play, for example, use of different aerosol models differentiated in size distribution function and refractive index.

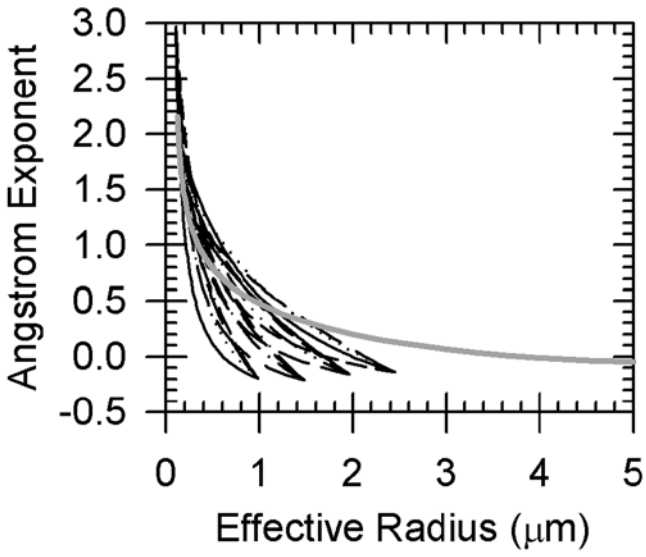

Figure 13. Ångström exponent versus effective radius for modified power size distributions (thick gray line) and for various combinations of bimodal size distributions (thin lines with various types). Each line stands for different combinations of small and large modes that compose bimodal lognormal size distributions.

[35] The MODIS retrieval algorithm employs 20 combinations of aerosol size distributions given by bi–log normal (BL) functions with variable refractive index. The GACP/AVHRR algorithm used a modified power (MP) law size distribution with a fixed refractive index. Extensive model simulations were conducted to investigate the impact of the differences in the size distribution function and the refractive index on the AOT discrepancies. It is found that the difference in the size distribution function can bring about substantial AOT discrepancies of up to a factor of 2, while different refractive indices cause a moderate systematic difference. The discrepancies depend on the similarity in aerosol size modes selected by the two algorithms. More drastic underestimations of AOT by the GACP/AVHRR relative to the MODIS is more likely induced by the differences in cloud screening including misclassification of heavy aerosols as clouds in the GACP/AVHRR product. Thus more attention should be paid to aerosol size distributions in addition to refractive index and cloud screening. The noisiness of the GACP/AVHRR aerosol retrievals is partially affected by the radiometric uncertainty of the AVHRR radiances, but it is unlikely to explain the large systematic discrepancies between the MODIS and GACP/AVHRR AOTs.

[36] Larger discrepancies exist in the Ångström exponent (α) derived from the MODIS and the GACP/AVHRR. The GACP/AVHRR retrievals seem to suffer from random-like errors with low signal-to-noise ratio. In comparison, the MODIS α product is of better quality in terms of spatial

variation and its correlation with the AOT. We attempted to understand the discrepancies between α derived from the MODIS and the AVHRR by modeling the effects of aerosol size distribution function, wavelength selection, and refractive indices on α retrieval. While errors in the α retrieval originate from numerous sources (e.g., selection of different wavelength pairs can cause a difference in α of up to 0.5), our model simulations also point to a big contribution by different aerosol models used in the AVHRR and MODIS retrieval algorithms. The influence of aerosol size distribution on the estimation of aerosol effective radius from α is also evaluated. For a given α, the corresponding aerosol effective radii may differ by more than 1 μm among the various size distribution functions.

[37] **Acknowledgments.** We thank the GACP, MODIS and AERONET aerosol teams at NASA GISS and GSFC for their great endeavors by processing and providing the aerosol products. We are also grateful to Goddard DAAC and MODIS software development and support team for processing, archiving and distributing the satellite data. This study is supported under grants provided by DOE, NASA, ONR, and NSF: DEFG0201ER63166, NGT530475/NNG04GE79G, N0001402IP20018, and ATM0425069, respectively.

References

Ångström, A. (1929), On the atmospheric transmission of Sun radiation and on dust in the air, *Geogr. Ann.*, *12*, 130–159.

Ångström, A. (1964), The parameters of atmospheric turbidity, *Tellus*, *16*, 64–75.

Brest, C. L., W. B. Rossow, and M. D. Roiter (1997), Update of radiance calibrations for ISCCP, *J. Atmos. Oceanic Technol.*, *14*, 1091–1109.

Charlson, R. J., S. E. Schwartz, J. M. Hales, R. D. Cess, J. A. Coakley Jr., J. E. Hansen, and P. J. Hoffman (1992), Climate forcing of anthropogenic aerosols, *Science*, *255*, 423–430.

Chou, M.-D., P.-K. Chan, and M. Wang (2002), Aerosol radiative forcing derived from SeaWiFS-retrieved aerosol optical properties, *J. Atmos. Sci.*, *59*(3), 748–757.

Chu, D. A., Y. J. Kaufman, C. Ichoku, L. A. Remer, D. Tanré, and B. N. Holben (2002), Validation of MODIS aerosol optical depth retrieval over land, *Geophys. Res. Lett.*, *29*(12), 8007, doi:10.1029/2001GL013205.

Chylek, P., B. Henderson, and M. Mishchenko (2003), Aerosol radiative forcing and the accuracy of satellite aerosol optical depth retrieval, *J. Geophys. Res.*, *108*(D24), 4764, doi:10.1029/2003JD004044.

Coakley, J. A., Jr., R. L. Bernstein, and P. A. Durkee (1987), Effects of ship stack effluents on cloud reflectance, *Science*, *237*, 953–1084.

Cox, C., and W. Munk (1954), Statistics of the sea surface derived from Sun glitter, *J. Mar. Res.*, *13*, 198–227.

Deuzé, J. L., P. Goloub, M. Herman, A. Marchand, G. Perry, S. Susana, and D. Tanré (2000), Estimate of the aerosol properties over the ocean with POLDER, *J. Geophys. Res.*, *105*, 15,329–15,346.

Dubovik, O., B. Holben, T. F. Eck, A. Smirnov, Y. J. Kaufman, M. D. King, D. Tanré, and I. Slutsker (2002), Variability of absorption and optical properties of key aerosol types observed in worldwide locations, *J. Atmos. Sci.*, *59*, 590–608.

Eck, T. F., B. N. Holben, J. S. Reid, O. Dubovik, A. Smirnov, N. T. O'Neill, I. Slutsker, and S. Kinne (1999), Wavelength dependence of the optical depth of biomass burning, urban, and desert dust aerosols, *J. Geophys. Res.*, *104*(D24), 31,333–31,349.

Eck, T. F., et al. (2003), Variability of biomass burning aerosol optical characteristics in southern Africa during the SAFARI 2000 dry season campaign and a comparison of single scattering albedo estimates from radiometric measurements, *J. Geophys. Res.*, *108*(D13), 8477, doi:10.1029/2002JD002321.

Geogdzhayev, I. V., M. I. Mishchenko, W. B. Rossow, B. Cairns, and A. A. Lacis (2002), Global two-channel AVHRR retrievals of aerosol properties over the ocean for the period of NOAA-9 observations and preliminary retrievals using NOAA-7 and NOAA-11 data, *J. Atmos. Sci.*, *59*(3), 262–278.

Goloub, P., D. Tanré, J. L. Deuzé, M. Herman, A. Marchand, and F.-M. Breon (1999), Validation of the first algorithm applied for deriving the aerosol properties over the ocean using the POLDER/ADEOS measurements, *IEEE Trans. Geosci. Remote Sens.*, *37*, 1586–1596.

Haywood, J. M., P. N. Francis, I. Geogdzhayev, M. Mishchenko, and R. Frey (2001), Comparison of Saharan dust aerosol optical depths retrieved using aircraft mounted pyranometers and 2-channel AVHRR algorithms, *Geophys. Res. Lett.*, *28*(12), 2393–2396.

Herman, J. R., P. K. Bhartia, O. Torres, C. Hsu, C. Seftor, and E. Celarier (1997), Global distribution of UV-absorbing aerosols from Nimbus 7/TOMS data, *J. Geophys. Res.*, *102*(D14), 16,911–16,922.

Higurashi, A., and T. Nakajima (1999), Development of a two-channel aerosol retrieval algorithm on a global scale using NOAA AVHRR, *J. Atmos. Sci.*, *56*, 924–941.

Holben, B. N., T. F. Eck, and R. S. Fraser (1991), Temporal and spatial variability of aerosol optical depth in the Sahel region in relation to vegetation remote sensing, *Int. J. Remote Sens.*, *12*, 1147–1163.

Holben, B. N., et al. (1998), AERONET—A federated instrument network and data archive for aerosol characterization, *Remote Sens. Environ.*, *66*, 1–16.

Holben, B. N., et al. (2001), An emerging ground-based aerosol climatology: Aerosol optical depth from AERONET, *J. Geophys. Res.*, *106*(D11), 12,067–12,097.

Husar, R. B., J. M. Prospero, and L. L. Stowe (1997), Characterization of tropospheric aerosols over the oceans with the NOAA advanced very high resolution radiometer optical thickness operational product, *J. Geophys. Res.*, *102*, 16,889–16,909.

Ichoku, C., D. A. Chu, S. Mattoo, Y. J. Kaufman, L. A. Remer, D. Tanré, I. Slutsker, and B. N. Holben (2002), A spatio-temporal approach for global validation and analysis of MODIS aerosol products, *Geophys. Res. Lett.*, *29*(12), 8006, doi:10.1029/2001GL013206.

Ichoku, C., L. A. Remer, Y. J. Kaufman, R. Levy, D. A. Chu, D. Tanré, and B. N. Holben (2003), MODIS observation of aerosols and estimation of aerosol radiative forcing over southern Africa during SAFARI 2000, *J. Geophys. Res.*, *108*(D13), 8499, doi:10.1029/2002JD002366.

Ignatov, A., and N. R. Nalli (2002), Aerosol retrievals from multi-year multi-satellite AVHR Pathfinder Atmosphere (PATMOS) data set for correcting remotely sensed sea surface temperatures, *J. Atmos. Oceanic Technol.*, *19*, 1986–2008.

Ignatov, A., and L. Stowe (2000), Physical basis, premises, and self-consistency checks of aerosol retrievals from TRMM VIRS, *J. Appl. Meteorol.*, *39*, 2259–2277.

Ignatov, A., and L. Stowe (2002a), Aerosol retrievals from individual AVHRR channels. Part I: Retrieval algorithm and transition from Dave to 6S radiative transfer model, *J. Atmos. Sci.*, *59*, 313–334.

Ignatov, A., and L. Stowe (2002b), Aerosol retrievals from individual AVHRR channels. Part II: Quality control, probability distribution functions, information content, and consistency checks of retrievals, *J. Atmos. Sci.*, *59*, 335–362.

Ignatov, A., L. Stowe, and R. Singh (1998), Sensitivity study of the Ångström exponent derived from AVHRR over oceans, *Adv. Space Res.*, *21*, 439–442.

Ignatov, A., J. Sapper, S. Cox, I. Laszlo, N. R. Nalli, and K. B. Kidwell (2004), Operational aerosol observations (AEROBS) from AVHRR/3 on board NOAA-KLM satellites, *J. Atmos. Oceanic Technol.*, *21*, 3–25.

Iqbal, M. (1983), *An Introduction to Solar Radiation*, 390 pp., Elsevier, New York.

Jeong, M.-J., and Z. Li (2005), Quality, compatibility, and synergy analyses of global aerosol products of global aerosol products derived from the advanced very high resolution radiometer and Total Ozone Mapping Spectrometer, *J. Geophys. Res.*, doi:10.1029/2004JD004647, in press.

Kahn, R., P. Banerjee, D. McDonald, and D. J. Diner (1998), Sensitivity of multiangle imaging to aerosol optical depth and to pure-particle size distribution and composition over ocean, *J. Geophys. Res.*, *103*, 32,195–32,213.

Kahn, R., P. Banerjee, and D. McDonald (2001), Sensitivity of multiangle imaging to natural mixtures of aerosols over ocean, *J. Geophys. Res.*, *106*, 18,219–18,238.

Kaufman, Y. J., and B. N. Holben (1996), Hemispherical backscattering by biomass burning and sulfate particles derived from sky measurements, *J. Geophys. Res.*, *101*, 19,433–19,445.

Kaufman, Y. J., A. Gitelson, A. Karnieli, E. Ganor, R. S. Fraser, T. Nakajima, S. Mattoo, and B. N. Holben (1994), Size distribution and phase function of aerosol particles retrieved from sky brightness measurements, *J. Geophys. Res.*, *99*, 10,341–10,356.

Kaufman, Y. J., D. Tanré, L. A. Remer, E. F. Vermote, A. Chu, and B. N. Holben (1997), Operational remote sensing of tropospheric aerosol over land from EOS Moderate Resolution Imaging Spectroradiometer, *J. Geophys. Res.*, *102*(D14), 17,051–17,067.

Kaufman, Y. J., et al. (1998), Smoke, Clouds and Radiation-Brazil (SCAR-B) experiment, *J. Geophys. Res.*, *103*, 31,783–31,808.

Kaufman, Y. J., D. Tanré, and O. Boucher (2002), A satellite view of aerosols in the climate system, *Nature*, *419*, 215–223.

King, M. D., Y. Kaufman, D. Tanré, and T. Nakajima (1999), Remote sensing of tropospheric aerosols from space: Past, present, and future, *Bull. Am. Meteorol. Soc.*, *11*, 2229–2259.

Kinne, S. et al. (2001), How well do aerosol retrievals from satellites and representation in global circulation models match ground-based AERONET aerosol statistics?, in *Remote Sensing and Climate Modeling: Synergies and Limitations*, edited by M. Beniston and M. M. Verstraete, pp. 103–158, Springer, New York.

Levy, R. C., L. A. Remer, D. Tanré, Y. J. Kaufman, C. Ichoku, B. N. Holben, J. M. Livingston, P. B. Russell, and H. Maring (2003), Evaluation of the Moderate Resolution Imaging Spectroradiometer (MODIS) retrievals of dust aerosol over the ocean during PRIDE, *J. Geophys. Res.*, *108*(D19), 8594, doi:10.1029/2002JD002460.

Maring, H., D. L. Savoie, M. A. Izaguirre, L. Custals, and J. S. Reid (2003), Mineral dust aerosol size distribution change during atmospheric transport, *J. Geophys. Res.*, *108*(D19), 8592, doi:10.1029/2002JD002536.

Martins, J. V., D. Tanré, L. Remer, Y. Kaufman, S. Mattoo, and R. Levy (2002), MODIS cloud screening for remote sensing of aerosols over oceans using spatial variability, *Geophys. Res. Lett.*, *29*(12), 8009, doi:10.1029/2001GL013252.

McClatchey, R. A., R. W. Fenn, J. E. A. Selby, F. E. Volz, and J. S. Garing (1972), Optical properties of the atmosphere, *Rep. AFCRL-72-0497*, 110 pp., Air Force Cambridge Res. Lab., Hanscom Air Force Base, Mass.

Mishchenko, M. I., I. V. Geogdzhayev, B. Cairns, W. B. Rossow, and A. A. Lacis (1999), Aerosol retrievals over the ocean by use of channels 1 and 2 AVHRR data: Sensitivity analysis and preliminary results, *Appl. Opt.*, *38*, 7325–7341.

Mishchenko, M. I., I. V. Geogdzhayev, L. Liu, J. A. Ogren, A. A. Lacis, W. B. Rossow, J. W. Hovenier, H. Volten, and O. Munoz (2003), Aerosol retrievals from AVHRR radiances: Effects of particle nonsphericity and absorption and an updated long-term global climatology of aerosol properties, *J. Quant. Spectrosc. Radiat. Transfer*, *79–80*, 953–972.

Moorthy, K. K., S. S. Babu, and S. K. Satheesh (2003), Aerosol spectral optical depths over the Bay of Bengal: Role of transport, *Geophys. Res. Lett.*, *30*(5), 1249, doi:10.1029/2002GL016520.

Myhre, G., et al. (2004), Intercomparison of satellite retrieved aerosol optical depth over ocean, *J. Atmos. Sci.*, *61*, 499–513.

Nakajima, T., and A. Higurashi (1998), A use of two-channel radiances for an aerosol characterization from space, *Geophys. Res. Lett.*, *25*(20), 3815–3818.

Nakajima, T., A. Higurashi, K. Kawamoto, and J. E. Penner (2001), A possible correlation between satellite-derived cloud and aerosol microphysical parameters, *Geophys. Res. Lett.*, *28*(7), 1171–1174.

O'Neill, N. T., and A. Royer (1993), Extraction of bimodal aerosol-size distribution radii from spectral and angular slope (Ångström) coefficients, *Appl. Opt.*, *32*, 1642–1645.

O'Neill, N. T., T. F. Eck, B. N. Holben, A. Smirnov, A. Royer, and Z. Li (2002), Optical properties of boreal forest fire smoke derived from Sun photometry, *J. Geophys. Res.*, *107*(D11), 4125, doi:10.1029/2001JD000877.

Rao, C. R. N., L. Stowe, and P. McClain (1989), Remote sensing of aerosols over oceans using AVHRR data: Theory, practice and applications, *Int. J. Remote Sens.*, *10*, 743–749.

Reid, J. S., T. F. Eck, S. A. Christopher, P. V. Hobbs, and B. Holben (1999), Use of the Ångström exponent to estimate the variability of optical and physical properties of aging smoke particles in Brazil, *J. Geophys. Res.*, *104*(D22), 27,473–27,479.

Remer, L. A., et al. (2002), Validation of MODIS aerosol retrieval over ocean, *Geophys. Res. Lett.*, *29*(12), 8008, doi:10.1029/2001GL013204.

Remer, L., et al. (2005), The MODIS aerosol algorithm, products and validation, *J. Atmos. Sci.*, in press.

Ricchiazzi, P., S. Yang, C. Gautier, and D. Sowle (1998), SBDART: A research and teaching software toll for plane-parallel radiative transfer in the earth's atmosphere, *Bull. Am. Meteorol. Soc.*, *79*(10), 2101–2114.

Rossow, W. B., and L. C. Garder (1993), Cloud detection using satellite measurements of infrared and visible radiances for ISCCP, *J. Clim.*, *6*, 2341–2369.

Rossow, W. B., and R. A. Schiffer (1999), Advances in understanding clouds from ISCCP, *Bull. Am. Meteorol. Soc.*, *80*, 2261–2287.

Sakerin, S. M., and D. M. Kabanov (2002), Spatial inhomogeneities and the spectral behavior of atmospheric aerosol optical depth over the Atlantic Ocean, *J. Atmos. Sci.*, *59*(3), 484–500.

Stowe, L. L., A. M. Ignatov, and R. R. Singh (1997), Development, validation, and potential enhancements to the second-generation operational aerosol product at the National Environmental Satellite, Data, and Information Service of the National Oceanic and Atmospheric Administration, *J. Geophys. Res.*, *102*, 16,923–16,934.

Tanré, D., C. Deroo, P. Duhaut, M. Herman, J. J. Morcrette, J. Perbos, and P. Y. Deschamps (1990), Description of a computer code to simulate the satellite signal in the solar spectrum: The 5S code, *Int. J. Remote Sens.*, *11*, 659–668.

Tanré, D., Y. J. Kaufman, M. Herman, and S. Mattoo (1997), Remote sensing of aerosol properties over oceans using the MODIS/EOS spectral radiances, *J. Geophys. Res.*, *102*(D14), 16,971–16,988.

Torres, O., P. K. Bhartia, J. R. Herman, Z. Ahmad, and J. Gleason (1998), Derivation of aerosol properties from satellite measurements of backscattered ultraviolet radiation: Theoretical basis, *J. Geophys. Res.*, *103*(D14), 17,099–17,110.

Torres, O., P. K. Bhartia, J. R. Herman, A. Sinyuk, P. Ginoux, and B. Holben (2002), A long-term record of aerosol optical depth from TOMS observations and comparison to AERONET measurements, *J. Atmos. Sci.*, *59*, 398–413.

Twomey, S. A., M. Piepgrass, and T. L. Wolfe (1984), An assessment of the impact of pollution on the global albedo, *Tellus, Ser. B*, *36*, 356–366.

Wang, M., and H. R. Gordon (1994), Radiance reflected from the ocean-atmosphere system: Synthesis from individual components of the aerosols size distribution, *Appl. Opt.*, *33*, 7088–7095.

Whitby, K. Y. (1978), The physical characteristics of sulfur aerosols, *Atmos. Environ.*, *12*, 135–159.

D. A. Chu, Laboratory for Atmospheres, NASA Goddard Space Flight Center, Code 913, Greenbelt, MD 20771, USA. (achu@climate.gsfc.nasa.gov)

M.-J. Jeong and Z. Li, Department of Meteorology and Earth System Science Interdisciplinary Center, University of Maryland, College Park, MD 20742, USA. (mjeong@atmos.umd.edu; zli@atmos.umd.edu)

S.-C. Tsay, Laboratory for Atmospheres, NASA Goddard Space Flight Center, Code 916, Greenbelt, MD 20771, USA. (tsay@climate.gsfc.nasa.gov)